Int. J. of GEOMATE, Sept., 2013, Vol. 5, No. 1 (Sl. No. 9), pp. 620-627
Geotec., Const. Mat. & Env., ISSN:2186-2982(P), 2186-2990(O), Japan

COLLAPSIBILITY IN CALCAREOUS CLAYEY LOESS: A FACTOR OF STRESS-HYDRAULIC HISTORY

Arya Assadi Langroudi[1] and Ian Jefferson[2]
[1,2]School of Civil Engineering, University of Birmingham, United Kingdom

ABSTRACT: The re-use of excavated loess in embankments needs a good understanding of its long-term mechanical response. Among the many collapse controlling factors, stress and hydraulic history are of significant importance as certain combination of these can alter the packing state to great extents. However, published works on stress path-packing state interaction is limited to clayey silts, underreporting the contribution of carbonates. Works on hydraulic path-packing state interaction lacks physical evidences for pore distribution, leading to disputes over the variation of air-volume over time and therefore fills' long-term behaviour. Identical artificial loess specimens were incrementally stressed on dry-, wet-, and wetting-surfaces, while microfabric, suction, particle and pore size distribution were recorded. The response of test material (moderately calcareous lightly clayey silt) showed the failure of dry-compaction in restricting the coefficient of consolidation. Wetting at any stress level improved the pore volumes and thus post-drying collapsibility. However, pre-loading to 25kPa before flooding provided the maximum degree of densification. Water-retention properties were deemed reproducible upon wetting-drying seasons for minimum content of 5-20μm size loess constituents. In short, controlled stress-hydraulic paths can guarantee the long-term response of site-won loess embankments.

Keywords: Loess, Collapsibility, Packing, Hydraulic Hysteresis, Stress History

1. INTRODUCTION

Any type of soil can collapse (sudden reduction in volume) under the correct stress/hydraulic conditions. Loess in particular is an iconic collapsible soil that covers about 10% of earth's landmass. This area is draped from Western Europe to China, and patchily covers North America, central Africa, and Australia. Loess may lose the cementation and suddenly collapse upon loading and/or wetting. Collapse results in a range of hazards, scaling from ground subsidence in urban areas to differential settlements under vertical storage tanks, pipelines, roads and rail tracks. Damage to buildings (e.g. Nevada USA in [1], slopes (e.g. north-west China in [2]), coastlines (e.g. Rissa Quick Clay, Norway in [3]), water conveyance structures and irrigation canals (e.g. Tashkent district Tajikistan in [4]), airport runways (e.g. Heathrow UK in [5, 6]), earth-dams (e.g. Teton Dam in Idaho USA, in [7]), road embankments (e.g. Iowa USA in [8]), and industrial installations (e.g. Russia in [9] and North Kazakhstan in [10]) as a result of collapse, are broadly reported in the literature. Loess research in geotechnical theme generally aims to understand the controlling factors and mechanism of collapse, and to use these to mitigate the collapse or to re-use the poor site-won loess in fills and embankments.

A handful of factors control the collapsibility of loess deposits: Freezing and ice growth develops the abundance of pore spaces, aggregation of clays and therefore collapsibility. Thawing results in dispersion and illuvial migration of fines in depths and formation of loose clay bridges [11]. Depending on the particle size and stress levels, wetting may either result in flocculation, softening and destruction of metastable fabrics, or leaching and decalcification. Drying may develop a negative pore water pressure, which draws clay fragments into the grains' contacts. Drying may also contribute in the precipitation of carbonates ([11,12], which increases the collapsibility. Solifluction is responsible for the formation of reworked loess. Solifluction may disrupt clay buttresses and cryogenic fabrics [13] and form more stable structures [14]. Ecological changes may decrease the collapsibility by formation of nodular calcretes after erosion of roots [11,15], bio-mineralization [16], algae photo-synthesis [17], and bacterial Ureolysis [18]. Collapsibility however may slightly increase through sulphate uptake by vegetation in wetlands. Temperature gradients may also slightly increase the collapsibility through chemical weathering and silica impregnation [19]. Contamination slightly alters the collapsibility through oxidation-reduction [20], protonation-deprotonation, and zeolition. Major contributions in the quantitative interaction between stress and packing state are reported in the works of [22, 23]. However, these are limited to clayey silt loess soils (e.g. significance of clay flake association in [21]), since few published works, if any, considers the contribution of carbonates. Suction-packing interaction also received much attention in literature within the framework of microfabric-associated effective stress models. Early attempts concern the simplified single porosity concepts. Works of [24]

(single fluid), [25] (two immiscible fluids), and [26] (two miscible fluids) fall into this category. More recent works concern the double porosity concept, highlighting the interaction of collapse, microfabric, effective stress and suction [27-29]. However, the theoretical theme of these works lacks physical evidences for the multi-porosity features of loess. This is the reason behind the much dispute over the specific pore-size scales for which the hydraulic hysteresis properties of loess is reproducible. In addition, the uncertainties with suction-packing interaction give space to the dispute over the variation of air volume (i.e. available space to collapse) in loess over time.

The present work investigates the contribution of hydraulic and stress history in collapsibility of calcareous loess, since these are the main controlling factors during embankments' service life. Suction-controlled oedometer tests were conducted on identical artificial loess specimens, containing moderate contents of carbonates and low contents of clay (see below section 2.1). Packing state was defined as the spatial relative arrangement of solids and void in a soil domain. In this context, solids' size distribution in conjunction with the fraction of domain's void volume controlled the pore size distribution. This made the packing state parameters equivalent to: particle size distribution, pore size distribution, micro-fabric and void ratio. Particle size distribution was derived by Laser Diffraction Spectroscopy. Micro-fabric images were produced by the use of an environmental scanning electron microscopy. Arya-Paris Pedo-transfer function [30] was applied to measure the pore-size distribution. Reading the trend of void ratio against net stress and matric suction in conjunction with the four packing indexes clarified: (1) the control of stress history on micro-mechanism of wetted-collapse, (2) the control of hydraulic history on micro-mechanism of stressing-induced collapse, (3) the control of carbonates before, during, and after the wetted-collapse, (4) the control of packing indexes on hydraulic hysteresis reproducibility and thus long-term seasonal collapse.

2. MATERIALS AND TESTING METHODS

2.1 Sample Preparation

Artificial moderately calcareous lightly clayey silt loess was used as a representative of typical loess soil. Test specimens contained 70% (by mass) quartz silt, 10% kaolinite and 20% carbonates (see Fig 1), including burbankite (anhydrous carbonate), vaterite (calcium carbonate), calcium carbonate hydrate, aragonite, calcium chloride, calcium carbide, defernite and sodium chloride.

The engineering of artificial loess included simulation of provenance (silt formation), depositional, consolidation, and post-depositional events. Primary clay and secondary salt crystals formed after depositional events. A change of packing from the initial unstable to metastable state took place after slight consolidation. Secondary clayey bonds and medium-soluble carbonate bonds formed by the end of the simulated post-depositional event.

To imitate the Periglacial quartz size reduction during the late Pleistocene and Halocene geological eras, Leighton Buzzard Sand was crushed in a high-energy Siebtechnik disc mill for 10 grinding phases each lasting 1 minute. Half a minute cooling time was considered between any two grinding events. A combination of fatigue and fracturing breakage led to the formation of dust of 10-20μm pronounced mode size. Series of sedimentation experiments (i.e. the use of Stoke's law) was undertaken to fit the dust into 2 to 63μm size range (provenance events). Oven-dried silt, clay, and anhydrous sodium carbonate powder were then crumbled and mixed thoroughly. This simulated the dry cryoturbation prior to free-fall aeolian deposition. The mix was pluviated into a standard 75mm oedometer ring from a constant height of 400mm via a nozzle. Distilled water was subsequently sprayed over the top surface of each 2-mm thick freshly deposited layer. This simulated the deposition of dry dust on confronting with a wet-trap (e.g. wetlands). Sequences were continued to form a deposited column of 27.5mm high (depositional events). Samples were then consolidated under 12.5kPa pressure (K_0 condition) for two hours. Consolidation simulated the solifluction/erosion of surface layers or the retreat of the ice during the early interglacial era. Lightly over-consolidated samples were then gently dried at the temperature of 75 to 85°C for 72 hours, to imitate the semi-arid climate. Afterwards, dried samples were exposed to capillary rise of 0.4M $CaCl_2$ aqueous solution (pH=8.0 to 9.0) for 9 hours at 25°C, to simulate the ingress of high dielectric melt-water into the soil. Saturated samples were then dried at 75 to 85°C for 24 hours. In total, three wetting-drying cycles were implemented. Test specimens were finally oven-dried at 110°C for 24 hours (post-depositional events), before the mechanical test.

2.2 Mechanical Testing

Oedometer tests were conducted in three phases. In the first phase, suction was decreased under zero external stress and under varying stresses. In the second phase, identical specimens of varying wetting-stresses (i.e. stress at which soil is flooded) were incrementally (standard fashion [31]) stressed to 2100kPa. In the last phase, identical specimens were stressed on the dry-surface. Packing state indexes were probed against stress (or wetting time).

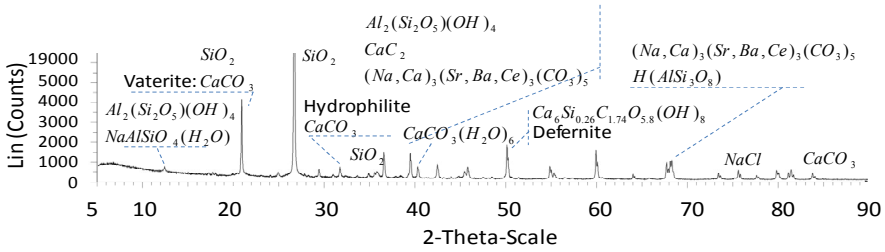

Fig 1. X-ray Diffraction Micro-graph

On the dry curve, each loading increment was retained for a minimum of 1 hour. On the wet curve, this minimum time was increased to four hours to satisfy the primary consolidation.

To investigate the suction-packing interaction, a standard filter paper test [32] was conducted on cubic specimens of 20mm and 10mm width and 20mm height. Target water contents were attempted to increase step-wise in 5-7% increments, starting from soil's hygroscopic moisture content (0.1%) up to 30.5% in 6 stages. Wetting was continued to approach the saturation water content (39.4%). An equilibrium time of 8 days was considered adequate for each stage [33].

2.3 Analytical Techniques

The Laser Diffraction (LD) analysis was applied over the 0.4µm to 2mm size range (i.e. the machine's range). For the micronization process, 4g of crumbled grains were fed into the vibrating channel with 0.5mm free-fall distance. Grains were then passed through the jet milling channel at 4.0 bar gas pressure. The machine provides cumulative distribution using the third quartile (Q3) of a normal distribution (at 99.73% degree of confidence).

To study the pore size distribution, Arya-Paris model was employed [30], [34-36]. The consistency of model with loess was examined in [37] on Chinese Loess Plateau deposits. The work advised the cautious application of method with soils of high clay or coarse-grained contents, or of a bimodal grading. With the low 10% clay content, absence of >60µm particles and unimodal particle size distribution (at 20µm), test material satisfied technique's limitations (see [30], [34-36]). The cumulative particle size distribution curve was divided into 14 fractions, with boundaries at 2, 3, 4, 5, 6, 7, 8, 9, 10, 20, 30, 40, 50, 60 and 63µm grain diameters. With each discrete domain, the pore volume, volumetric water content, abundance of spherical particles, length of the cylindrical pore space, mean pore radius and the equivalent soil water pressure was calculated. A detailed account of model's formulation is discussed in [30]. Scaling parameter was selected in accordance with the 'texture dependent' method of 'logistic growth curve in [36] (latest modifying update of model, presented by the function developers).

3. RESULTS AND DISCUSSION

3.1 Wetting

3.1.1 Wetting under Zero External Net Stress

A pronounced reduction in the mass of 5-20µm grains upon wetting is recorded in LD graphs (Fig 2). This suggests that a remarkable quota of sub-20µm grains coagulated into larger assemblages on wetting. In other words, the tendency for coagulation (i.e. or aggregation) reduced in >20µm and <5µm particles.

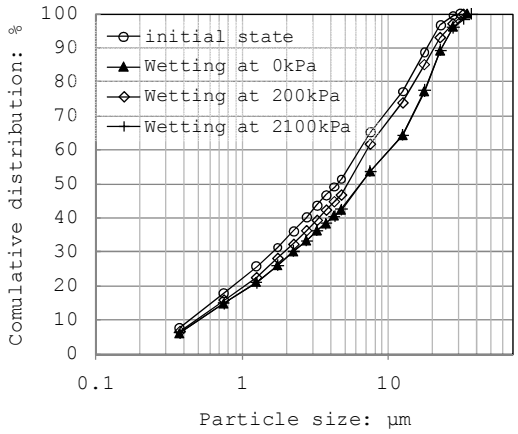

Fig 2. Particle size distribution on suction decrease surface

The $(PP_i\text{-}PP_W)/PP_i$ ratio is plotted against particle size in Fig 3, where: PP_i is the passing percent of grains through a given mesh opening size before wetting, and PP_W is the passing percent of grains through a given mesh opening size after wetting.

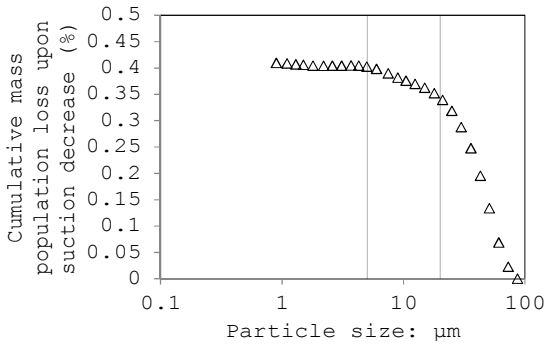

Fig 3. Cumulative population loss upon suction decrease at zero net stress

Higher values of $(PP_i\text{-}PP_W)/PP_i$ indicate stronger aggregation. In Fig 3, signature of constant but

strong aggregation is showed in sub-5µm grains. Aggregation slightly decreased for 5-20µm grains. A sharp reduction in aggregation took place with increasing grain size from 20µm to 87µm. The plot highlights the significance of sub 20µm particle loss upon wetting. The change in particles' population is commented in Table 1 after reading Fig 2 in conjunction with Fig 3.

Table 1. Contribution of wetting in changing the mass of particles with certain size

Particle size: µm	Population (mass):%
0.35	Loss of 40%
0.35 to 5	Loss of 40%
5	Loss of 40%
5 to 20	Loss of 40% to 34%
20 to 87	Loss of 34% to 0%

Fig 4 (commented in Table 2) shows the dynamics of pore size distribution on wetting for varied wetting stresses (i.e. hydraulic history).

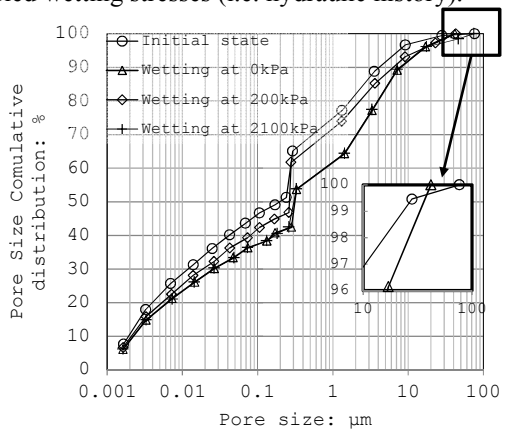

Fig 4. Pore size distribution on suction decrease surface

Table 2. Contribution of wetting in changing the volume of pore spaces with certain size

Pore size: µm	Population (volume)
0.001	Minimum loss
0.001 to 0.25	Degree of loss improving at slow rate
0.25 to 0.3	No change
0.3 to 1.5	Some high degree of loss, lesser at 1.5µm
1.5 to 8	Sharp reduction in loss (lowest at 8µm)
8 to 19	Some high degree of loss, lesser at 19µm
19 to >19	Sharp reduction in loss (negligible at >19µm)

The decrease in the volume of fine pore spaces (0.001 to 0.25 and 0.3 to 1.5µm) and the marginal drop in the volume of large pore spaces (1.5 to 8, and >19µm) highlighted the aggregation in sub 20µm particles. Fig 5 shows three qualities of fabric in clay, silt, and carbonate-rich domains.

The maximum pore size dropped from 76 to 42µm on wetting (Fig 4). Reduced pore size gave rise to the curvature radii's and thus decreased the suction. This agrees with the hysteresis effect (Fig 6).

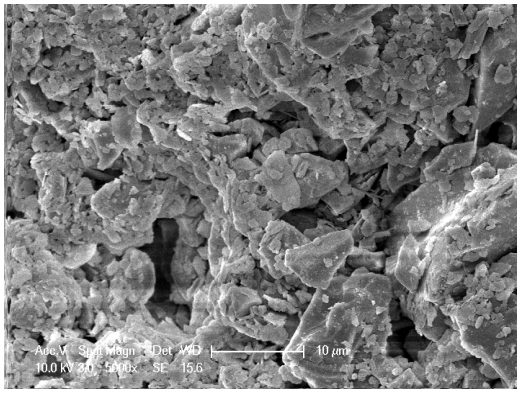

Fig 5-a. Coagulation in carbonate-rich clusters

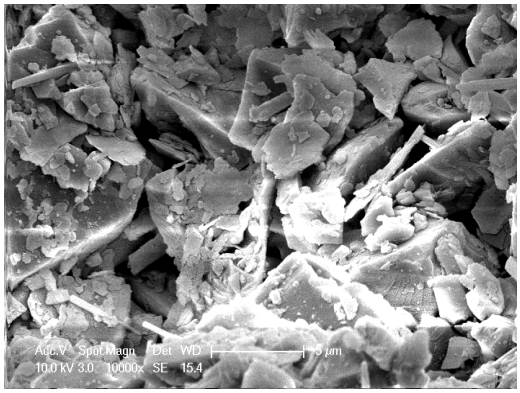

Fig 5-b. Coagulation in clay-rich clusters

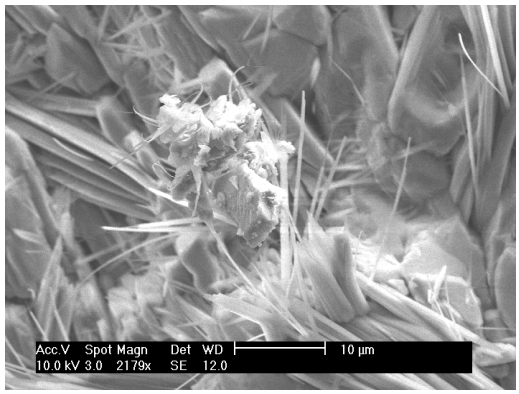

Fig 5-c. Coagulation in silt-rich clusters

Hydraulic hysteresis is linked to the association of micro-fabric and soils' affinity for water, thus any change to particles and pore size arrangements allows the hydraulic hysteresis to take place. On this basis, 5 to 20µm gains, and 0.001 to 0.25µm as well as 0.3 to 1.5µm in diameter pores were deemed responsible for the hydraulic hysteresis. This agrees with the work of [33] on French calcareous loess, consisting of 80-85% silt (of 20µm mode) and 15% Calcium Carbonate, which showed matrix clusters of relatively low pore size and population were most sensitive to the water content changes.

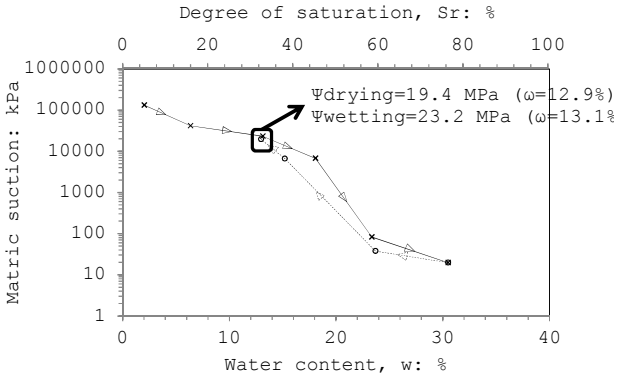

Fig 6. SWCC curve derived after filter paper test

3.1.2 Wetting under Varying External Net Stress

In presence of an external net stress, which was high enough to maximize the skeletal forces but low enough to preserve the pores, wetting caused the maximum collapse volume change (Fig 7). Coefficient of collapsibility in Fig 7 was determined for varying flooding stresses and is given by $C_{col} = \Delta e/(1+e_1)$, where Δe is the wetting-induced decrease in void ratio; and e_1 is pre-wetting void ratio. C_{col} is normalized against the initial void ratio (before stressing and/or wetting), to allow the comparison between identical specimens.

20% carbonates appeared as poor macro-pore bracing units (fig 5-c) and strong inter-silt bridge connectors (Fig 13-a), while the relatively minor 10% clay appeared as clayey coats for silt, beneath the external carbonate shield (Fig 5-b) and aggregates at the macro-pore space (Fig 10-b). Clay therefore has a relatively minor contribution to the collapse mechanism.

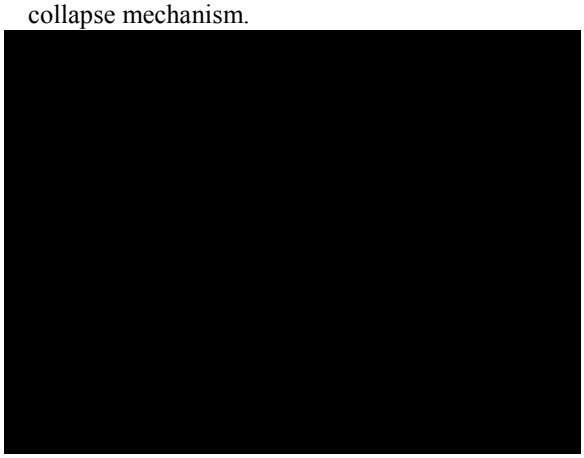

Fig 7. Norm C_{col} vs. flooding pressure: kPa

Wetting released the inter-particle connectors (through physical washing and mechanical shearing). Particles approached to contact points (asperities) by the driving force of gravity and stored skeletal forces. Higher skeletal forces induce higher grain-to-grain impact forces and thus more crushed grains (Fig 8). The reduction in skeletal force with increasing flooding stress allowed the coagulation (section 3.1.1) to develop. This countered the size reduction effect at stress levels as high as 1600kPa (Fig 7).

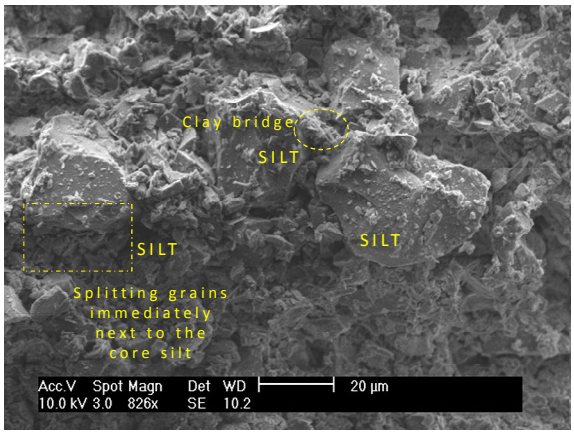

Fig 8. Grain crush and edge chipping caused by wetting

To realize what range of particle sizes were most affected by coagulation, the $(PP_i\text{-}PP_W)/PP_i$ ratio was plotted against particle size in Fig 9 for the flooding stress of 2100kPa. In Fig 9, coagulation took place at both clay-size (sub 1µm) and silt-size (20-30µm). Reading the loss of 1µm particles in conjunction with microscopic images (Fig 10) revealed the migration of clay from contact points to the macro-pores. Silt- and clay-size crushed quartz also migrated with clay/carbonates into the macro-pores.

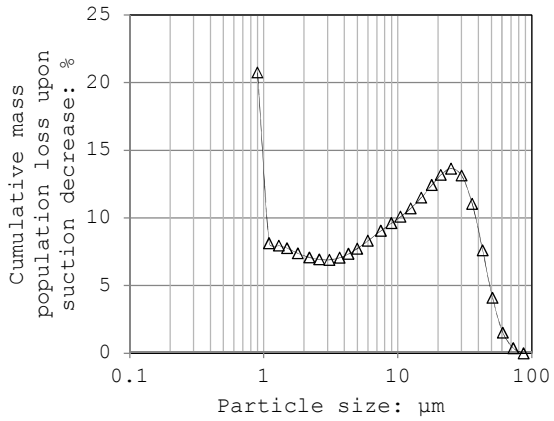

Fig 9. Cumulative particles' population loss upon wetting at 2100kPa net stress

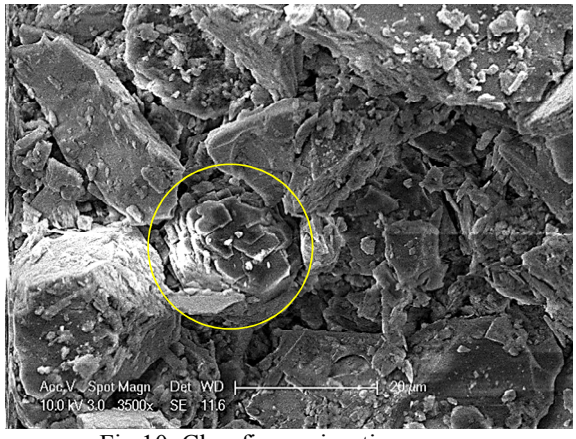

Fig 10. Clay-fines migration

From a different perspective, some tubular carbonates re-precipitated in a scaffolding framework and formed re-stored bridges (Fig 11). This induced a residual post-wetting collapsibility.

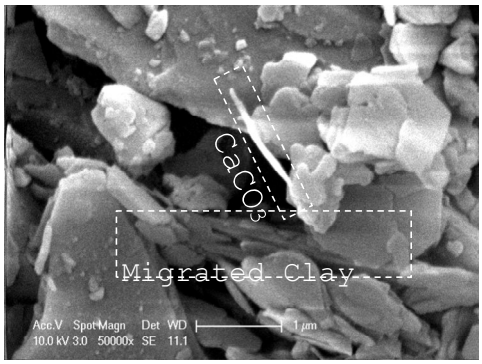

Fig 11. Tubular carbonate bridges after flooding

3.2 Dry Stress-State Surface

K_0-stressing triggered the packing change by compressing 0.8 to 20μm silts into connectors. This was evidenced with early reduction in population of sub 20-μm particles (Fig 12).

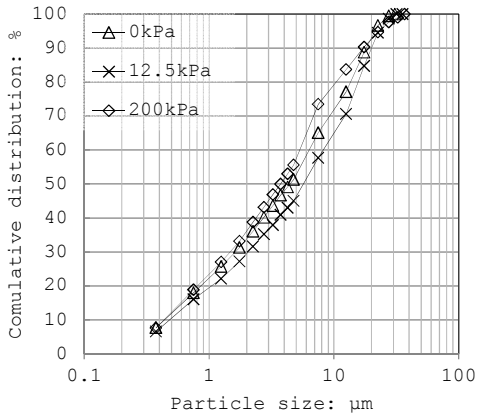

Fig 12. Particle size distribution on dry surface

Early changes to packing state were associated with grains' re-arrangement rather than collapse. Buttress units survived under relatively low levels of skeletal forces. Assemblages took a dispersed association and the size of clusters slightly decreased (Fig 13 and 14): Four assemblage units are shown in hatched lines in Fig 13-a. Within each assemblage unit, chains of silt-bond-silt surround macro-pores. This is schematically illustrated in Fig 13-a. In Fig 13-b (post-stressing re-arranged assemblage), silt chains arch macro-pore spaces of reduced volume. This is schematically illustrated in Fig 14.

Further increase in net stress to 200kPa led to the breakage of silt grains. This was reflected in increased mass of 1 to 20μm grains (Fig 12). Crushing continued but with a decelerating rate with increasing net stress to 2100kPa (Fig 15).

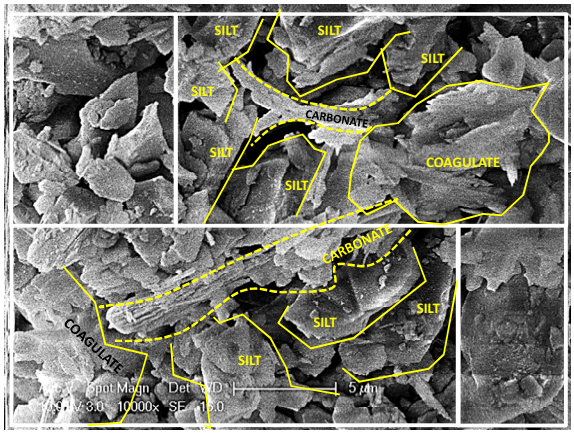

Fig 13-a. Initial packing (before compression)

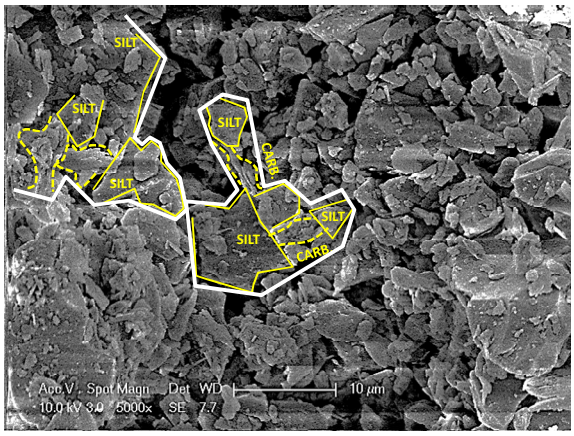

Fig 13-b. Post-stressing packing

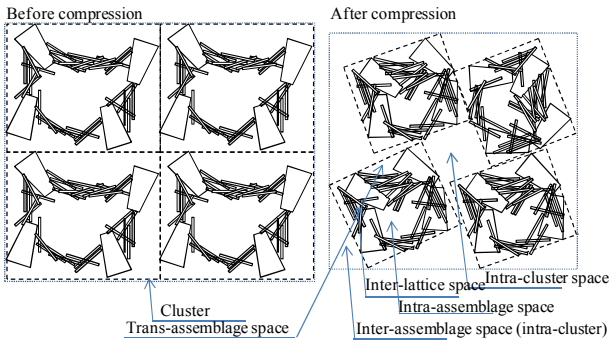

Fig 14. Schematic of particle arrangement before and after constant water content compression

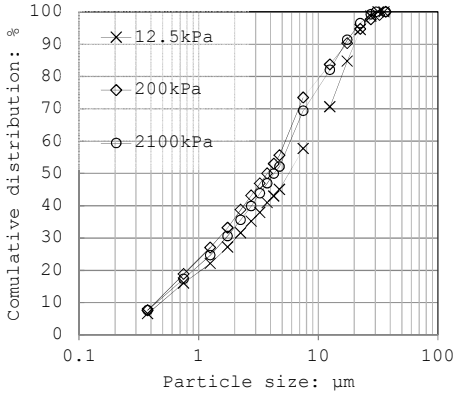

Fig 15. Particle size distribution on dry surface

With reference to Fig 16, a multi-modal pore size distribution was obtained for stress levels beyond 200kPa. From a micromechanical perspective, soil medium consists of a number of clusters, each containing assemblages of silts bonding together with carbonate/clay (Fig 14). Upon stressing to 2100kPa, trans-assemblage pore spaces were destroyed due to air expulsion. This is mirrored in the decrease in population of 0.25 to 2μm pore spaces (Fig 16). Silt grains were forced into the buttress units, which reduced the intra-assemblage pore spaces. This implements the drop in the population of 0.001 to 0.25μm void spaces. Clusters rotated and approached to contact points, forming new inter-assemblage pore spaces. The increase in abundance of 2 to 20μm pores was attributed to the formation of these inter-assemblage spaces.

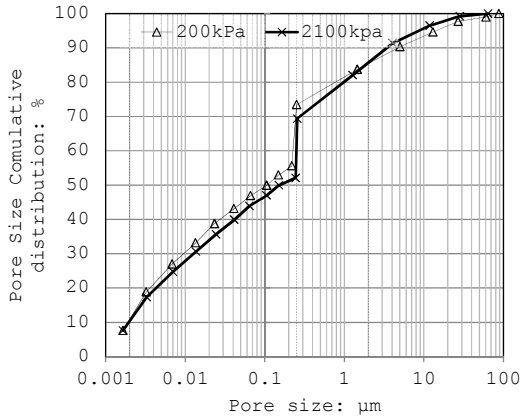

Fig 16. Pore size distribution on dry-surface

3.3 Wet Stress-State Surface

The dynamics of packing state on the wet-surface shall be viewed in the light of stress-hydraulic history. The $(e_f-e_0)/e_0$ is plotted against the flooding pressure in Figure 17, where e_f is the void ratio at 2100kpa under saturated condition and e_0 is the void ratio before stressing at the dry state.

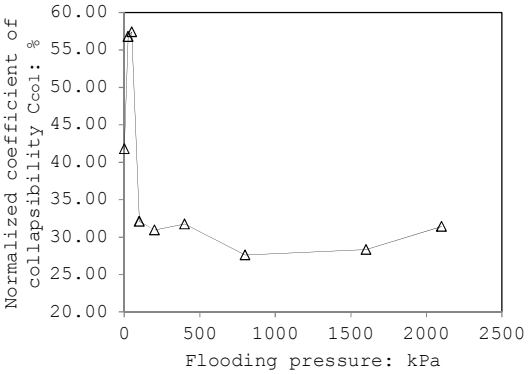

Fig 17. Plot of mean normalized contraction volume change at 2100kpa against flooding pressure

The enhanced consolidation for 12.5kPa flooding stress is due to the maximum content of collapse upon wetting, the micromechanical grounds of which discussed earlier. Further increase in consolidation for 25kPa flooding stress is due to relatively high dry-state compression in addition to the high content of collapse upon wetting. From a different perspective, the marginal difference between the compressibility of specimen pairs on dry-state at 12.5 and 25kPa, and also the higher degrees of wetted collapse at 12.5kPa than 25kPa, highlighted the dependency of coefficient of volume compressibility (m_v) to the flooding pressure.

4. CONCLUSION

The micromechanical response of a typical loess soil (moderately calcareous lightly clayey silt) was studied on the dry-, wetting-, and wet stress-state surfaces. The study allowed a better understanding of collapse triggering mechanisms, and the interaction between stress/hydraulic path and packing state. Furthermore, the work provided physical evidence for the double porosity concept, by classifying the pore spaces into: micro-, macro- and transient levels.

The response of test material (moderately calcareous lightly clayey silt) showed the failure of dry-compaction in restricting the coefficient of consolidation. Wetting at any stress level improved the aggregation (in sub-30μm grains), pore volumes and thus post-drying collapsibility. However, pre-loading to 25kPa before flooding gave the maximum degree of densification. Water-retention properties are found reproducible upon wetting-drying seasons for minimum contents of 5-20μm size loess constituents. Hydraulic hysteresis was deemed restricted to pores ranging from 0.001 to 0.25μm and also 0.3 to 1.5μm diameter. In short, controlled stress-hydraulic paths can guarantee the long-term response of site-won loess embankments.

5. REFERENCES

[1] McMurdo, D. and P. Gomez, Rains, soils vex road crews, in Rahrump Valley Times. 2005: Nye County.

[2] Derbyshire E., X. Meng, and T.A. Dijkstra, Landslides in the thick terrain of north-west China. 2000, Chichester, West Sussex, England: John Wiley & Sons, Ltd.

[3] NGI. 1978 - Rissa Historical landslide 1978.

[4] Rogers, C.D.F., T.A. Dijkstra, and I.J. Smalley, Hydroconsolidation and subsidence of loess: Studies from China, Russia, North America and Europe: In memory of Jan Sajgalik. Engineering Geology, 1994. 37(2): p. 83-113.

[5] Rose, J., et al., Palaeoclimate, sedimentation and soil development during the Last Glacial Stage (Devensian), Heathrow Airport, London, UK. Quaternary Science Reviews, 2000. 19(9): p. 827-847.

[6] Jefferson, I.F., I.J. Smalley, and K.G. Northmore, Consequences of a modest loess fall over southern Britain. American Geologist, 2003. 15(4): p. 199-208.

[7] Smalley, I.A.N., The Teton Dam: rhyolite foundation + loess core = disaster. Geology Today, 1992. 8(1): p. 19-22.
[8] Handy, R.L., Collapsible loess in Iowa. Soil Science Society of America Journal, 1973. 37: p. 281-284.
[9] Askalonov, V.V., Silicatization of loess soils [in Russian] in Sokolivich, V. E., 1965, Silicatization of loess soils, Soil Mechanics and Foundation Engineering, Vol. 2 (1), pp. 3-7. Mashstroiizdat, 1949.
[10] Roohnavaz, C., E.J.F. Russell, and H.F. Taylor, Unsaturated loessial soils: a sustainable solution for earthworks. Proceedings of the Institution of Civil Engineers-Geotechnical Engineering, 2011. 164(4): p. 257-276.
[11] Milodowski, A.E., et al., The mineralogy and fabric of brickearths and their relationship to engineering properties Bulletin of Engineering Geology, In Press.
[12] Boardman, D.I., et al., Physico-chemical characteristics of British loess. Proceedings of the 15th Int'l Conference on Soil Mechanics and Geotechnical Engineering Vols 1-3. 2001, Leiden: A a Balkema Publishers. 39-42.
[13] Derbyshire, E. and T.W. Mellors, Geological and geotechnical characteristics of some loess soils from China and Britain - a comparison Engineering Geology, 1988. 25(2-4): p. 135-175.
[14] Pye, K., The nature, origin and accumulation of loess. Quaternary Science Reviews, 1995. 14(7-8): p. 653-667.
[15] Joseph, S. and K.P. Thrivikramaji, Rhizolithic calcrete in Teris, southern Tamil Nadu: Origin and paleoenvironmental implications. Journal of the Geological Society of India, 2005. 65(2): p. 158-168.
[16] Lowenstam, H.A. and S. Weiner, On biomineralization. 1989, New York: Oxford University Press.
[17] Dipova, N. and V. Doyuran, Assessment of the collapse mechanisms of tufa deposits. Engineering Geology, 2006. 83(4): p. 332-342.
[18] Chou, C.W., et al., Bacterially induced calcite precipitation via Ureolysis. 2008, American Society for Microbiology: Washington, USA.
[19] Krauskope, K.B., Dissolution and precipitation of silica at low temperatures. Geochimica et Cosmochimica Acta, 1956. 10: p. 1-26.
[20] Fukue, M., et al., Change in microstructure of soils due to natural mineralization. Applied Clay Science, 2003. 23(1-4): p. 169-177.
[21] Mitchell, J.K., Fundamentals of soil behaviour. 1976: Wiley.
[22] Nolan, G.T. and P.E. Kavanagh, Computer simulation of random packing of hard spheres. Powder Technology, 1992. 72(2): p. 149-155.
[23] Miller, H., Modelling the collapse of metastable loess soils 2002, Unpublished PhD thesis, The Nottingham Trent University.
[24] Terzaghi, K., The shear resistance of unsaturated soil, in 1st International Conference on Soil Mechanics and Foundation Engineering. 1936. p. 54-56.
[25] Bishop, The principle of effective stress. Teknisk Ukeblad, 1959. 106: p. 859-863.
[26] Matyas, E.L. and H.S. Rahakrishna, Volume change characteristics of partly saturated soils. Geotechnique, 1968. 18: p. 432-448.
[27] Khalili, N., et al., Effective stress in double porous media with two immiscible fluids. Geophysical Research Letters, 2005. 32 (L15309): p. 1-5.
[28] Bagherieh, A.R., et al., Drying response and effective stress in a double porosity aggregated soil. Engineering Geology, 2009. 105(1-2): p. 44-50.
[29] Alonso, E.E., et al., A microstructurally based effective stress for unsaturated soils. Geotechnique, 2010. 60(12): p. 913-925.
[30] Arya, L.M. and J.F. Paris, A physicoempirical model to predict the soil moiture characteristic from particle-size distribution and bulk density data. Soil Science of America Journal, 1981. 45: p. 1023-1030.
[31] BS1377-5, B., Methods of test for Soils for civil engineering purposes - Part 5: Compressibility, permeability and duribility tests. 1994, BSi.
[32] ASTM, standard test method for measurement of soil potential (suction) using filter paper, D 5298-03 2003, ASTM International: West Conshohocken, PA.
[33] Munoz-Castelblanco, J.A., et al., The water retention properties of a natural unsaturated loess from northern France. Geotechnique, 2012. 62(2): p. 95-106.
[34] Arya, L.M. and J.F. Paris, Reply to comments on: A physicoempirical model to predict the soil moisture characteristic from particle-size distribution and bulk density data. Soil Science Society of America Journal, 1982. 46: p. 1348.
[35] Haverkamp, R. and Parlange, Comments on: A physicoempirical model to predict the soil moisture characteristic from particle-size distribution and bulk density data. Soil Science Society of America Journal, 1982. 46: p.1348.
[36] Arya, L.M., et al., Scaling parameter to predict the soil water characteristic from particle-size distribution data. Soil Science Society of America Journal, 1999. 63: p. 210-519.
[37] Mingbin, H., D.G. Fredlund, and M.D. Fredlund, Estimation of SWCC from grain size distribution curves for loess soils in china, in 62nd Canadian Geotechnical Conference 2009: Halifax, NS, Canada.

Int. J. of GEOMATE, Sept., 2013, Vol. 5, No. 1 (Sl. No. 9), pp. 620-627.
MS No. 62312 received on May 29, 2013 and reviewed under GEOMATE publication policies.

Corresponding Author: Arya Assadi